SPACE CHARGE LENS FOR FOCUSING HEAVY ION BEAMS[*]

K. Schulte[†], M. Droba, O. Meusel, U. Ratzinger
Institute for Applied Physics, Goethe-University, Frankfurt a. M., Germany

Abstract

Space charge lenses use a confined electron cloud for the focusing of ion beams. Due to the electric space charge field, the focusing is independent of the particle mass. For this reason the application of space charge lenses especially in the field of heavy ion beams is advantageous. Moreover, the trapped non neutral plasma cloud compensates the space charge forces of the ion beam. The focusing strength is given by the confined electron density whereas the density distribution influences the mapping quality of the space charge lens. An important parameter for the focusing capability of the space charge lens besides the homogeneity is a high electron density. In ongoing theoretical and experimental work methods have been developed to determine the most important parameters like electron temperature and electron density distribution for an optimized lens design. Based on experimental results a new space charge lens has been designed to focus low energy heavy ion beams like a 2.2 keV/u U^{4+} at the low energy transport section into the GSI High Current Injector [1]. Experimental results will be presented in comparison with numerical simulations.

SPACE CHARGE LENS FOR THE HSI-UPGRADE

The beam transport of high perveance heavy ion beams is influenced by high space charge forces and high ion mass. The introduction of trapped electrons into the low energy beam transport section (LEBT) leads to space charge compensation and focusing of the ion beam at drastically reduced magnetic and electric field strength compared to conventional ion optics. The high current injector (HSI) at GSI provides experimental conditions to investigate the performance of the space charge lens. As an alternative LEBT concept which is described in [2] a new space charge lens has been designed for the possible application at the HSI upgrade.

The length of the prototype is 436 mm with an aperture of 150 mm (fig. 1). The device is optimized for a 2.2 keV/u U^{4+}-beam with a maximum beam radius of 50 mm. For the mapping quality of the space charge lens the electron density distribution due to the confining fields is very important. Numerical simulations by the use of Φ_A=30 kV electrode potential and the magnetic field of B_z=13 mT for the confinement of the non neutral plasma results in a nearly homogeneous electron density distribution of $n_{e,max}$=2.7·10^{14} m^{-3}. This yields a linear selffield
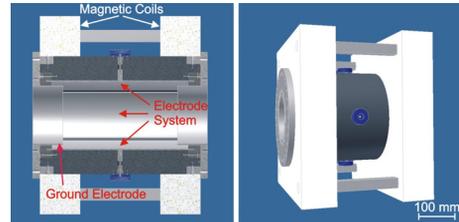

Figure 1: The design of the HSI lens prototype (B_{max}=0.1 T, $\Phi_{A,max}$=50 kV).

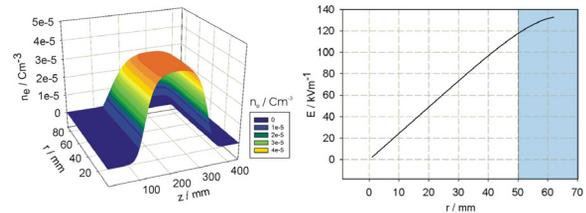of E_r=117 kV/m at r=50 mm (fig. 2). The magnetic field

Figure 2: Calculated electron density distribution (left) and the resulting radial electrostatic selffield of the non neutral plasma in the lens midplane (right).

produced by the coils is not uniform in the z direction. In comparison to an ideal homogeneous magnetic field it leads only to minor changes in the radial electron density distribution (fig. 3).
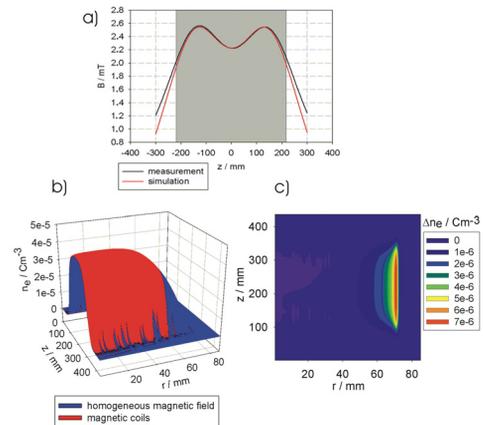

Figure 3: a) Measured (I=5A) and calculated magnetic field of the coil system, b) comparison of the electron density distribution, and c) difference of the electron density calculated for the homogeneous field and the field of the magnetic coils.

03 Technology

3H Other Technology

BEAM TRANSPORT SIMULATION

With respect to the design of the prototype the transport of a 2.2 keV/u U^{4+}-beam as a function of the beam radius was simulated using the code LINTRA [3]. For these calculations a homogeneous phase space distribution at the entrance of the beam line and a space charge compensation of 100% was assumed. Fig. 4 shows the beam envelope along the transport section that consists of a first drift section with different lengths, the space charge lens, and a second drift of 650 mm. The output emittance at the end of the second drift for different beam radii ($r_{1,beam}$=38 mm, $r_{2,beam}$=51 mm, $r_{3,beam}$=72 mm) is presented as well. As
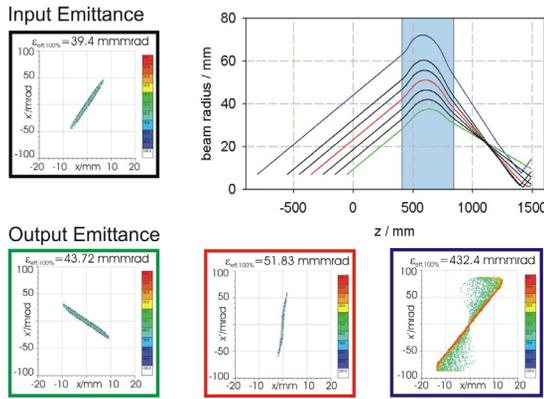

Figure 4: Beam envelope along the transport section, input emittance, and output emittance for selected beam radii.

a consequence of the linear electric field in radial direction aberrations only occur at the edge of the non neutral plasma column. At the edge of the electron cloud the density drops off over a distance on the order of the Debye length (λ_D=1.9 cm) which leads to an emittance growth (fig. 5). However, the emittance growth up to r_{beam}=58 mm
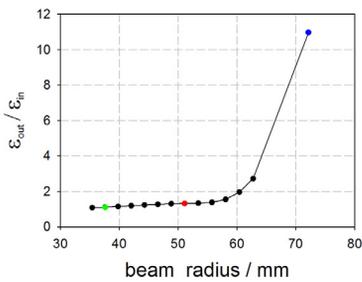

Figure 5: Emittance growth (100% ellipse) as a function of the beam radius. The colour code corresponds to the frames in fig. 4.

is below 2%. For an optimized lens design and in order to determine the operation mode the plasma parameters and the dynamics have to be further investigated experimentally.

03 Technology

3H Other Technology

DIAGNOSTICS AND EXPERIMENTS

To determine the important plasma parameters like electron temperature, electron density, and to investigate diagnostic techniques on a non neutral plasma three experimental setups have been established (fig. 6). In the following
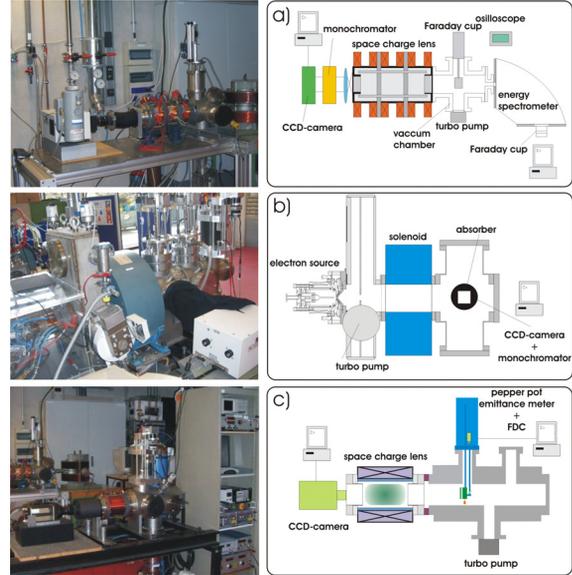

Figure 6: Experimental setup (not scaled) for a) density measurement, b) the study of optical technique to determine electron temperature, and c) pepperpot emittance measurement.

sections the methods to determine the plasma parameters are described.

Density Measurement

Within the lens volume the trapped electrons reduce the anode potential Φ_A and of course influence the electric field. The produced residual gas ions are accelerated within the electric field. The average electron density can be determined by measuring the ion energy with respect to the voltage drop the ions passed through [4]. The average electron density is given by:

$$\bar{n}_e = \frac{4\epsilon_0 \Delta\Phi}{er^2}, \qquad (1)$$

where $\Delta\Phi$ is the difference of the anode voltage and the voltage drop of ions, and r is the radius of the electrode. Measurements show that there are different regions of ion
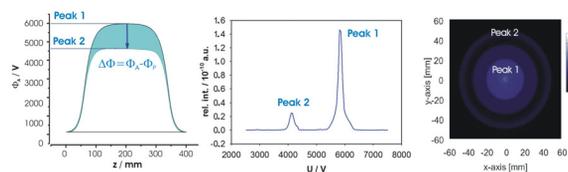

Figure 7: Scheme of the density measurement technique.

production within the electron plasma. This is also validated by numerical simulations (fig. 7). In determination of the average electron density the inner region (peak 1) plays an important role [5]. Peak 2 results due to the ion production in a small zone near the anode.

Temperature Measurement

Because of low electron densities ($n_e = 1 \cdot 10^{14}$ m^{-3}) and by absence of important recombination processes like three body recombination and radiative recombination the requirements for a typical temperature measurement are not fulfilled. The so called optical method relates the emitted line intensities to the cross section for production of excited states by the collision of an electron beam with residual gas like helium [6]. The direct cross section Q_j^d can be expressed by the optical-emission cross sections Q_{ji} and Q_{ki} as:

$$Q_j^d = \sum_i Q_{ji} - \sum_k Q_{ki}, \qquad (2)$$

$$Q_{ji} = \frac{I_{ji} e}{I n_0 t \Delta x}, \qquad (3)$$

where I_{ji} is the number of emitted photons, I the electron beam current, n_0 the target gas density, and Δx is the length of the electron beam region from which radiation is collected. The ratio of two cross sections of excited states in the helium atom is equal to the ratio of its emitted line intensities. Therefore it is possible to relate the intensity ratio to the electron energy. Fig. 8 shows the pressure de-
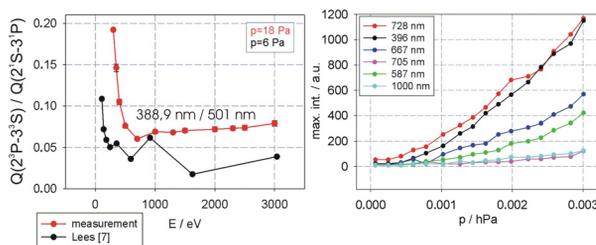
Figure 8: Measured ratio of the optical-emission cross section as a function of the electron energy and comparison to [7] (left), an example of pressure dependency of emitted line intensities (right).

pendency of the emitted line intensities respective the ratio of optical cross sections. This must be taken into account by the application of this method to determine the average kinetic energy of the electrons.

Pepperpot Emittance Measurement

The time-dependent field distribution within the space charge lens can be determined by the measurement of the transversal phase space of the emitted particles. Therefore, the time-resolved diagnostics by the pepperpot emittance scanner yields information about the plasma state [8]. Fig. 9 shows the result of the pepperpot emittance measure-
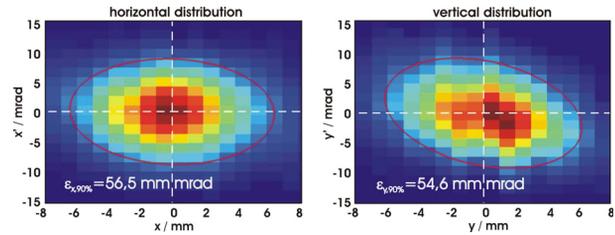
Figure 9: An example of measured transversal phase space distribution of emitted particles from the space charge lens.

ment behind the space charge lens after a drift of 80 mm. The parameters of the lens were B_z=8.3 mT for the confining magnetic field, potential Φ_A=2000 V on the anode, and the residual gas pressure of p=6$\cdot 10^{-5}$ hPa.

CONCLUSION AND OUTLOOK

The focusing of low energy heavy ion beams due to the design parameters of the space charge lens has been numerically investigated. A prototype that fulfills the requirements is under construction. Methods to determine the plasma parameters have been presented and will be further investigated. The next step will be the commissioning of the space charge lens and the determination of the operation mode with respect to the plasma parameters.

REFERENCES

[1] W. Barth, "The Injector Systems of the Fair Project", LINAC'08, Victoria, BC, Canada, MO204, p. 31, (2008), http://www.JACoW.org.

[2] A. Adonin et al., "Measurements of Transverse Ion Beam Emittance Generated by High Current Ion Sources at the GSI Test Injector facility HOSTI", Rev. Sci. Instrum. 81, 02B707 (2010).

[3] J. Pozimski and O. Meusel, "LINTRA ein Computerprogramm zur Berechnung des Strahltransportes teilkompensierter, hochperveanter Ionenstrahlen", GrakoNews, 1/1999, p. 33-34.

[4] K. Schulte et al., "Optical Diagnostic on Gabor Plasma Lenses", EPAC'08, Genoa, Italy, THPC104, p. 3221, (2008); http://www.JACoW.org.

[5] K. Schulte, "Untersuchung von Messmethoden zur Parameterbestimmung eines Nichtneutralen Plasmas", Diploma Thesis, Goethe-University, Frankfurt a. M., 2008, p. 53-54.

[6] A. R. Filipelli et al., "Principles and Methods for Measurement of Electron Impact Excitation Cross Sections for Atoms and Molecules by Optical Techniques", Advances in Atomic, Molecular, and Optical Physics, Vol. 33 (1994), p. 3-10.

[7] J. H. Lees, "The Excitation Function of Helium", H. H. Wills Physical Laboratory, University of Bristol, 1932, p. 173-186.

[8] J. Pfister, "Entwicklung und Anwendung schneller Strahldiagnose fuer Ionenstrahlen", PhD Thesis, Goethe-University, Frankfurt a. M., 2010, p. 120-122.